Verification and Measurement of Thrust Vectoring Using Thermal Mapping Techniques

Mark Y. Shapochka[1], Karl W. Roush[2], Andrew J. Yatsko[3], Dimitri N. Mavris[4]
Aerospace Systems Design Laboratory, Georgia Institute of Technology, Atlanta, GA, 30332

The feasibility of thrust vectoring measurement using thermal mapping techniques was investigated. In this study, thermal maps are represented by generated figures which display temperatures spatially using a grid of evenly spaced thermocouples. For the purpose of measurement of thrust vectoring, thermal maps as well as the distance from the engine nozzle exit to the thermocouple grid were used to triangulate the vectored angle. This investigation was intended to be conducted using a small gas turbine engine in instrumented experiments. The assessment of feasibility was based on cost analysis, as well as the accuracy of experimental results.

I. Introduction

In engine testing, one common method for thrust vector angle measurement has been to use load cells in the engine mount to record thrust force components and derive the thrust's angular displacement. Common thrust measurement techniques rely on load cells, often placed invasively on the engine, or require a larger experimental setup [1]. Research into thermal thrust vector measurement methods is not well documented, with those methods focusing on the thermal behavior of the TVC system [2]. In this research, exhaust thermal mapping for thrust vector measurement was studied, discovering whether substituting load cells with thermocouples provides accurate results. Accuracy was computed by comparing the results of the thermal map method with the physical angular displacement of the nozzle from in-line with the engine. Thermocouples were used to locate the position of the exhaust gas stream with time. The position data was used to triangulate the direction of the exhaust gas, allowing for the vector angle to be derived. To find the vector angle, the following method was planned to be followed: a thermocouple grid fixture would be assembled, MATLAB code to visualize test results and derive the vector angle would be generated, and instrumented tests using a small gas turbine engine would be conducted to discover the viability of this measurement method. Due to COVID-19, access to the engine was lost. Instead, experiments using a heat gun to replicate the exhaust stream of the engine were conducted. As a result, this research will provide documentation on the viability of alternative thrust vector measurement methods. The possible benefits of a thermal mapping method include reduced instrumentation costs, in comparison to common measurement methods, and less invasive implementation into existing experimental facilities.

II. Existing Thrust Vector Measurement Techniques

While computational methods do exist for simulating the effect of thrust vector control (TVC) devices [3], this paper focuses on the measuring TVC effects experimentally. Early attempts by NASA to measure varying thrust forces were accomplished by placing the engine inside of a movable carriage, which was then placed in a mounting ring. This mounting ring has load cells mounted along each axis. This system was very large and was only used to test the larger F100 derivative engines at NASA Lewis [4].

[1] Graduate Student, High-Speed Compressor Research Laboratory, Purdue University, AIAA Student Member.
[2] Graduate Student, Aerospace Systems Design Laboratory, Georgia Institute of Technology, AIAA Student Member.
[3] Research Engineer, School of Aerospace Engineering, Atlanta, GA, AIAA Senior Member.
[4] S.P. Langley NIA Distinguished Regents Prof., School of Aerospace Engineering, 270 Ferst Drive, Atlanta, GA, AIAA Fellow.

NASA's method has been adapted through mounting load cells around the body of the device, though the measurement equipment is still rather large and invasive [5]. More modern approaches follow the "equal but opposite reaction" principle, which allows for the force measurement devices to be mounted to a test plat opposite of the device [6]. An even less invasive method exists wherein the thrust is measured through the deflection of a flat component on the other end of the device, seen visually below.

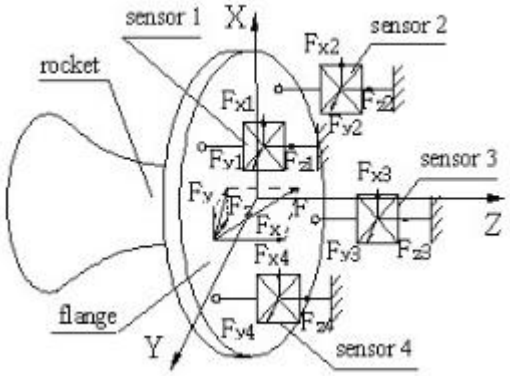

Fig. 1 Placement of thrust vector measurement for orbit/attitude rocket [7]

Looking at thermal techniques, there does not appear to be any precedent for using thermal mapping for thrust measurement purposes. Specifically, for TVC devices, thermal modeling is predominantly focused on how heat is transmitted to the system and how it is affected [2]- not how TVC devices modify the thermal properties of the exhaust stream.

III. Cost Analysis

One possible added benefit of a thermal mapping method is a cost advantage in comparison to load cell methods. To measure the thrust vector angle with load cells, a load cell ring must be positioned on the engine within the test stand, as shown in Fig. 2 labeled by "Sensor rod assembly".

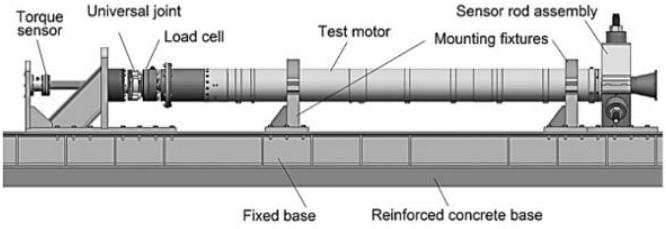

Fig. 2 Example of Engine Mounting with Load Cell Ring [1]

At least three load cells are needed to measure the deflection of thrust due to vectoring and quantify the thrust vector components in rectangular coordinates. A three-load cell configuration is shown in Fig. 3 below.

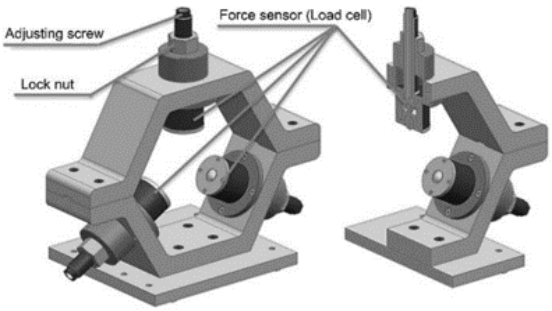

Fig. 3 Nozzle Load Cell Ring [1]

Four load cells can also be used for measurement, simplifying the calculations compared to the three-load cell system. When six load cells are used, seen in Fig. 4 below, a 6 degree-of-freedom load balance can be performed.

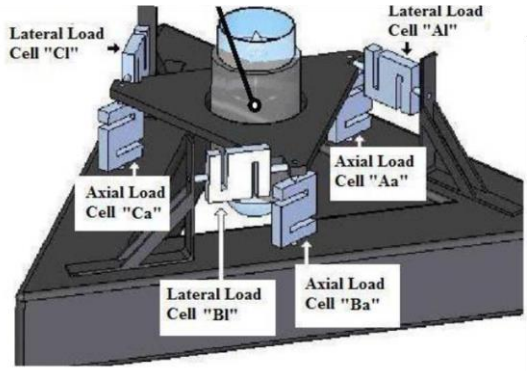

Fig. 4 Six Load Cell Configuration for 6 Degree-of-freedom Measurement [2]

The drawback of this measurement system is the fact that load cells are expensive. Expense here is understood as the cost of the measurement system relative to the cost of the engine being measured. In comparison to other measurement devices, one load cell can cost as much as about 53 individual thermocouple wires (comparison of 100 lbf Omega Miniature Load Cell [7] with Omega Thermocouple 5SRTC-GG-K-30-36 [9]). Thus, the exploration of other less-costly measurement methods was prudent.

The load cell used for cost comparison in this analysis was a 100 lbf Omega Miniature Load Cell, which cost $601.66 each [7]. In addition, the thermocouples used were Omega Thermocouples, 5SRTC-GG-K-30-36, which cost $11.64 per wire [9]. Next, the same data acquisition chassis was used for comparison, so that cost was included in the calculation. For load cells, the input module accounted for was the NI-9237 (C Series Strain/Bridge), which can handle inputs from up to four load cells and costs $1,625 [9]. Moreover, the module for thermocouple data acquisition was a combination of the NI-9210 ($375 [11]) and NI-9213 ($1,340 [12]). The NI-9210 can take an input of 4 thermocouples and the NI-9213 can take 16. To compare cost, as the price scales from three to six load cell configurations, as well as how many thermocouples are used per quadrant on a grid, Fig. 5 was generated.

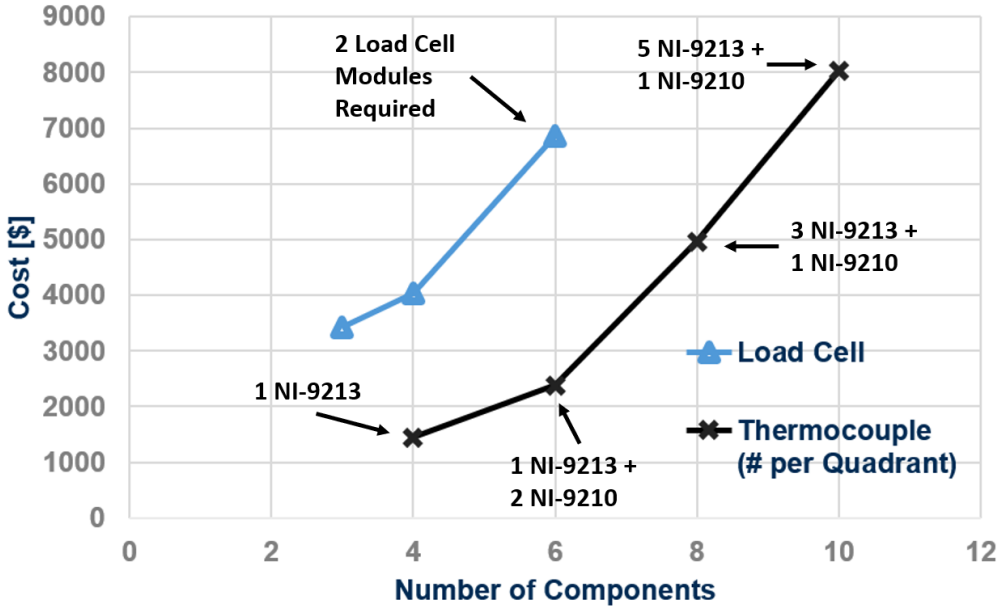

Fig. 5 Cost Scaling with number of sensors used

The horizontal axis in Fig. 5 represents the number of thermocouples or load cells used, while the vertical axis shows the total cost of each given combination of sensors and input modules. The captions denote what combination of input modules is required for each sensor amount. The thermocouple amounts represent groups of four, meaning 4 on the figure indicates 4 per quadrant, or 16 total thermocouples. The first two points on the load cell line include one load cell module and the corresponding number of load cells. The third point shows that another load cell module will be required to acquire data from all of the load cells used. As shown, there is a cost advantage to thermocouple measurement, apart from when 36 or more thermocouples are used.

The number of thermocouples used per quadrant on the grid will affect the spatial resolution of the thermal mapping. In addition, as an engine's nozzle increases in size, larger thermocouple grids will be required, increasing the number of thermocouples used per quadrant. The exact number of thermocouples used will also depend on the desired thermal map fidelity. For this study, 20 to 25 thermocouples will be used.

To study this problem, a JetCat P100 gas turbine engine with a modified vectoring nozzle was intended to be used, which costs $2,425. The P100 produces about 22.5 lbs of thrust, shown in Fig. 6.

Fig. 6 JetCat P100 Gas Turbine Engine [13]

As shown, substituting load cells with thermocouples presents significant savings. In terms of percent difference, a six thermocouple-per-quadrant grid is 30.6% cheaper than a three-load cell configuration. By the mentioned definition of expense, the 3-load cell configuration is expensive, as the cost is $1,004.98 more than the price of the engine itself, excluding the added cost of a data acquisition chassis.

IV. Experimentation

As mentioned, the engine's exhaust gas stream was tracked to derive the angle the nozzle has vectored. The stream was tracked by creating a thermal map of the gas temperatures a short distance from the nozzle exit. The exhaust stream was at a hotter temperature than the ambient air and thus was visible on the map. The figure below shows an example of a thermal map of an engine's exhaust.

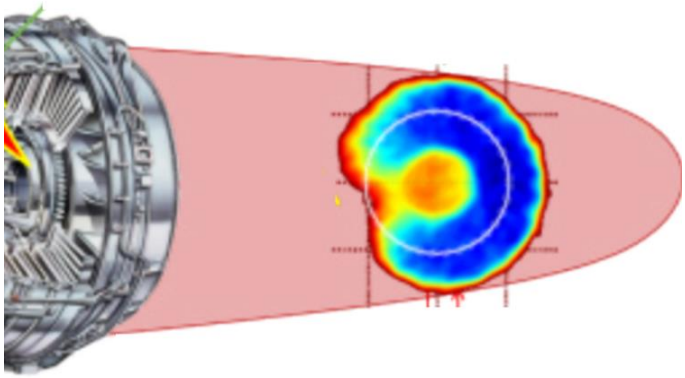

Fig. 7 Thermal Map of Engine Exhaust [14]

To measure the temperatures to populate the thermal map, a grid structure of uniformly inserted thermocouples was planned to be attached to the back end of the test stand used for JetCat P100 tests. This planned grid was substituted with an alternative grid, which will be discussed later in the paper. Fig. 8 below shows the test stand with the intended location of the thermocouple grid labeled. In addition, the distance from the grid to the nozzle would be fixed, represented in Fig. 9.

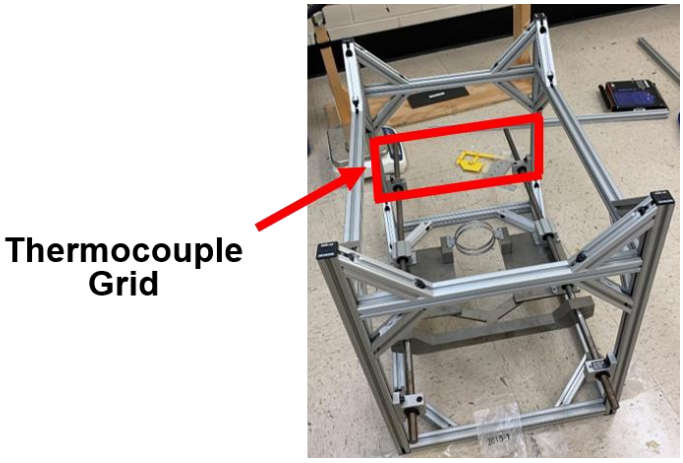

Fig. 8 Test Stand with location of Thermocouple Grid

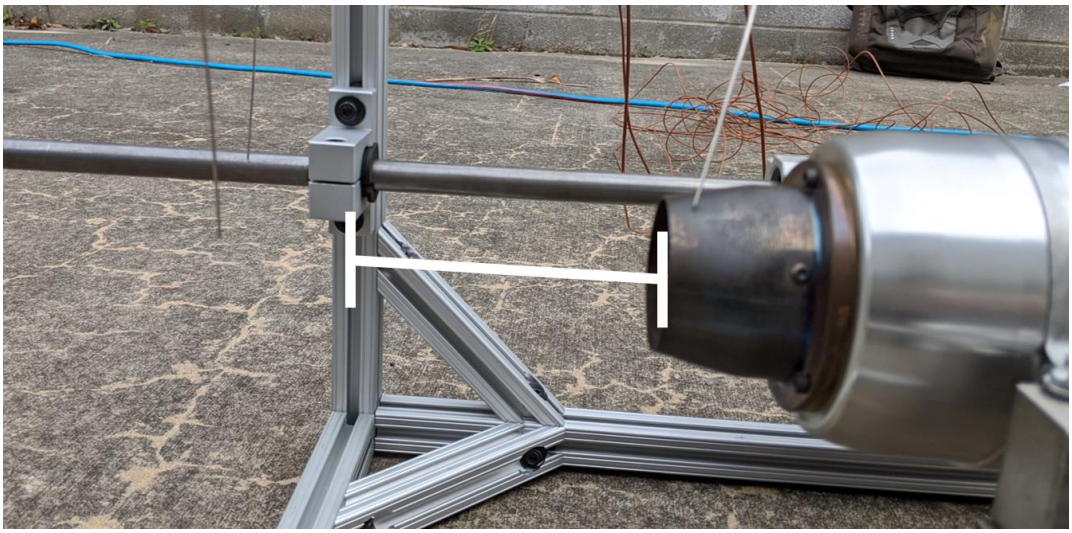

Fig. 9 Nozzle distance from Thermocouple Grid

During engine tests, using a thermocouple grid, the data acquisition system (DAQ) collected the temperature readings with time from each slot. Using this data, the data analysis script converted each temperature with time vector into a matrix of the temperature at the x,y positions of the corresponding slots. There is a matrix of temperatures at each coordinate for each time increment through the duration of the test. The figure below shows a sample of positions represented as coordinate points.

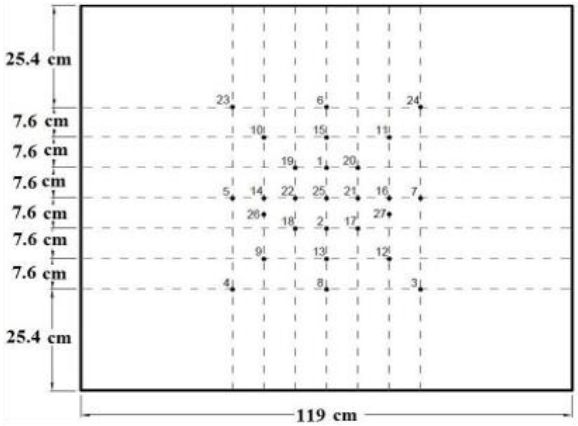

Fig. 10 Positions represented as Coordinate Points [15]

The thermocouple grid would fix to the test stand's aluminum extrusion bars and contain slots to secure each thermocouple to a constant coordinate position. The thermocouple wires to be used were insulated and the measuring end would be positioned out of the slot, so heat accumulated by the grid would not influence the thermocouple reading. The CAD rendering of the thermocouple grid is displayed in Fig. 11.

Fig. 11 Thermocouple Grid Rendering

Each thermocouple slot would have an insertion hole and an outlet hole to position the measuring wire end in the gas flow path. The slot's cross-section is shown below in Fig. 12.

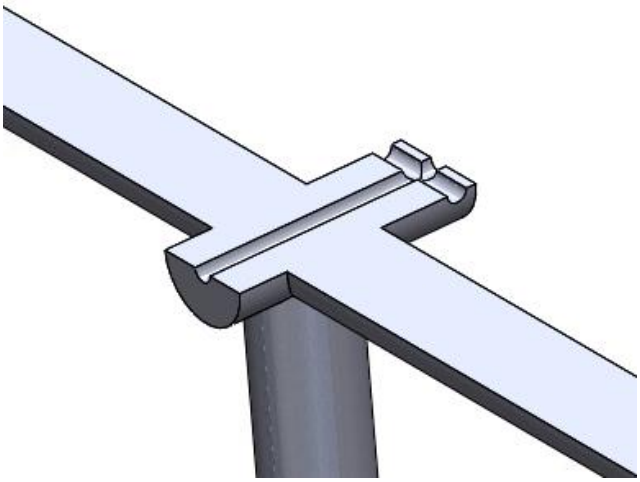

Fig. 12 Thermocouple Slot Cross-Section

Due to the outbreak of COVID-19, physical access to the test facilities at the Georgia Institute of Technology Aerospace Systems Design Laboratory and Combustion Laboratory was revoked. Therefore, the originally planned thermocouple grid was not assembled. In addition, the engine would not be available to be used for testing the thermocouple measurement system. As a result, a revised thermocouple grid would be constructed from readily available materials. Moreover, the exhaust flow of the engine would be replicated using a heat gun.

As shown in the figure below, the thermocouple grid was constructed using an aluminum frame with a steel wire grid. The grid spacing would be used to equally distribute the thermocouples spatially. The heat gun was mounted on a tri-pod for stable rotation during tests. For verification of the thermocouple-based calculation, a digital protractor was mounted on the top of the heat gun to measure the vertical rotation. In addition, to measure the horizontal rotation of the heat gun, the compass application on an iPhone 11 was used, which was connected to the side of the heat gun. The sensors mounted on the heat gun are shown in the figure below.

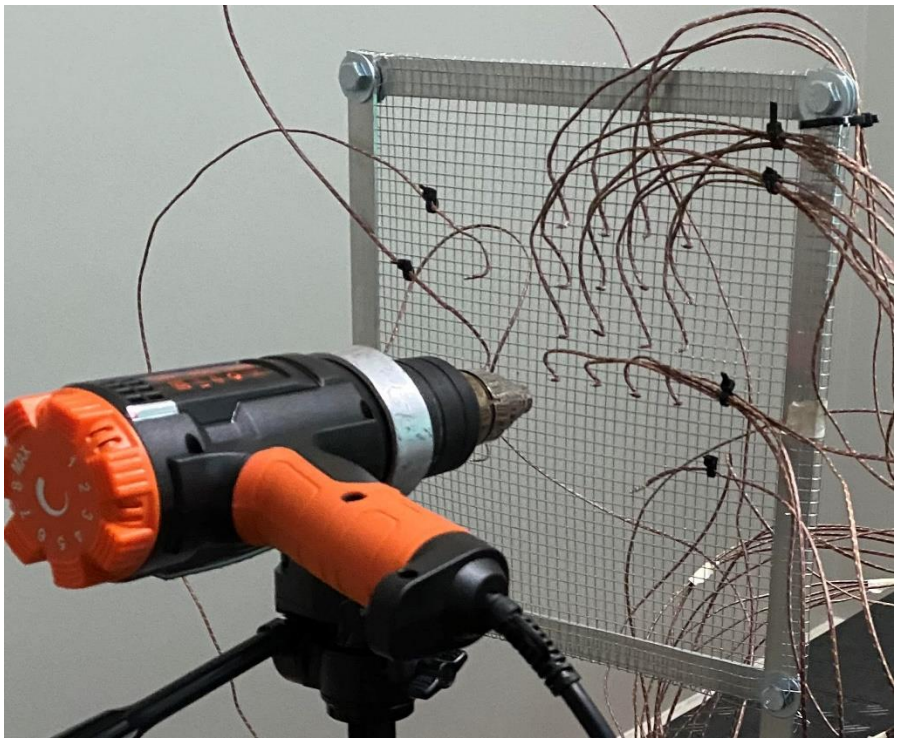

Fig. 13 Updated Thermocouple Grid with Heat Gun

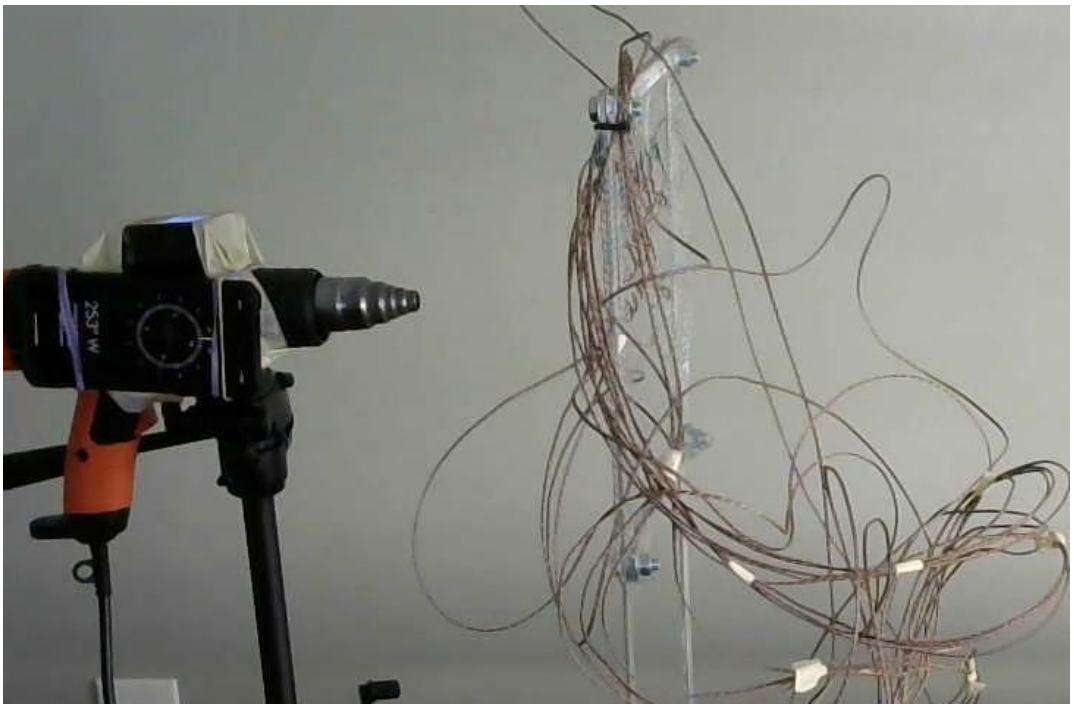

Fig. 14 Heat Gun with iPhone Compass and Digital Protractor for Angular Verification

V. Data Analysis

As mentioned, a MATLAB data analysis script was created to convert all the recorded temperatures with time into temperatures at x,y locations for each time step. The thermal map was created by plotting the temperature magnitude as a color from a scale for each x,y position in the map, using the MATLAB "imagesc" function. The spaces in the map between points were populated using the MATLAB matrix resize function (imresize) with bicubic weighted interpolation. A sample of the expected thermal map and scale is shown below.

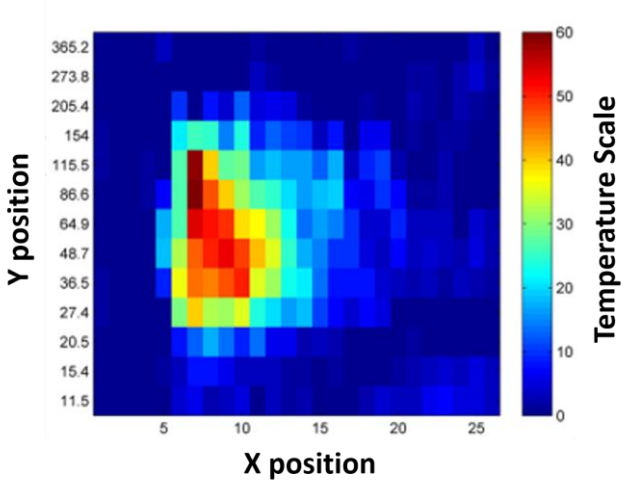

Fig. 15 Sample Thermal Map [16]

This thermal map was generated for each acquired data time increment. These maps were compiled into an animation showing the movement of the exhaust stream during vectoring. Using test data collected, a sample thermal map was generated. Two thermocouples were used, one in the exhaust gas stream and one at a slight offset in the ambient. The ambient temperature was repeated for all the grid locations except for the exhaust position. Using a preliminary version of the data analysis script, the following thermal map was produced:

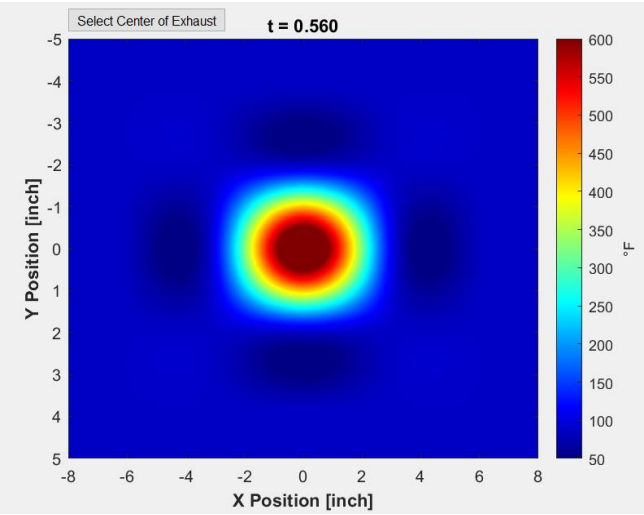

Fig. 16 Thermal Map using two Thermocouples

The derivation of the vector angle was made through the following sequence. First, the thermal maps of the nozzle in straight line and vectored positions were selected. Next, the thermal maps were compiled with time to form a video file [16]. While progressing through the time steps in the acquired data, once a sufficiently high temperature is reached, a white dot was plotted at the highest temperature measured. Following this, a magenta dot was plotted and tracked the highest point in the exhaust stream. During the entire animation creation, the magenta dot was used as the vectored center and denoted the X and Y distances from the origin. Following those steps, as the thermocouple grid's distance

from the nozzle was held constant, two triangles could be formed from the nozzle exit to the (0, 0) point and to the X and Y values of the second point. Finally, the angles with respect to the horizontal and vertical axes were quantified using the inverse tangents of the two triangles' component legs. To visualize the angle derivation, Figure 17 displays the located nozzle positions from the thermocouple grid measured temperatures. Figure 18 shows how the position data from the thermocouple grid is converted to vector angles.

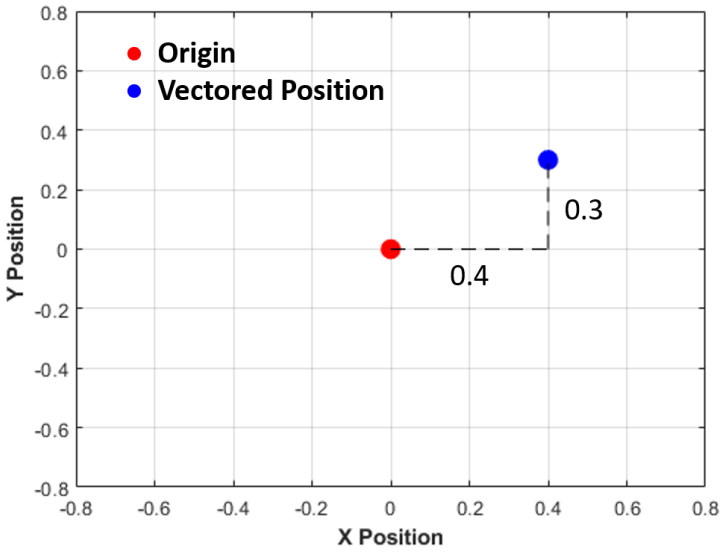

Fig. 17 Example of Nozzle Positions from Thermocouple Grid Measurements

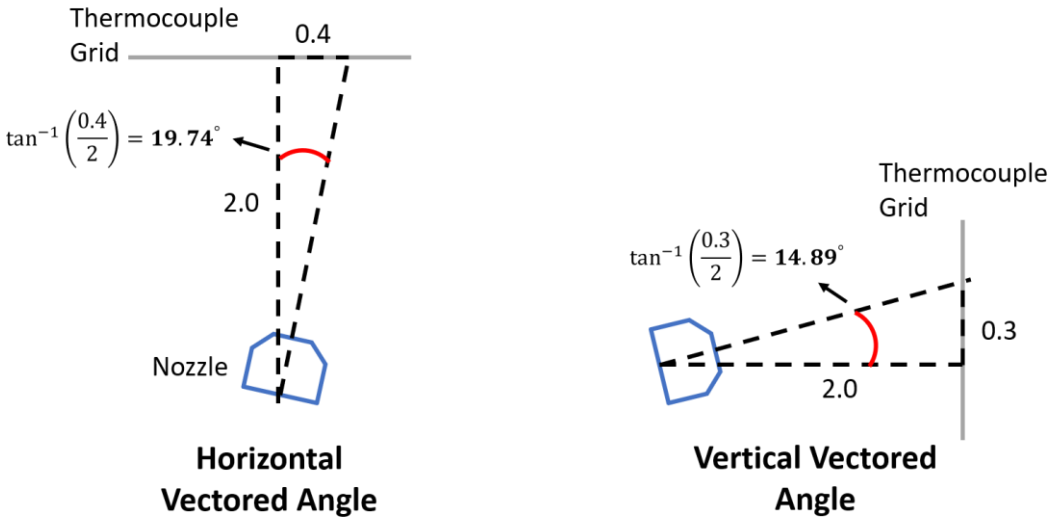

Fig. 18 Example of Conversion of Nozzle Positions into Vector Angles

During the animation, the dynamically calculated horizontal and vertical angles were shown on the generated figure. "Pause" and "Play" buttons were included to allow for the user to record any shown results of interest.

To quantify the accuracy of the thermal map method for thrust vector angle measurement, the experimental results were compared to other measurements of the angle traveled by the nozzle. As mentioned, a digital protractor measured the vertical angle travelled by the heat gun, while an iPhone compass showed the horizontal angle travelled.

VI. Results

To demonstrate the system and verify the accuracy of this measurement method, tests were conducted. As only 20 thermocouples were available to instrument the grid with, thermocouples were positioned in the following distribution.

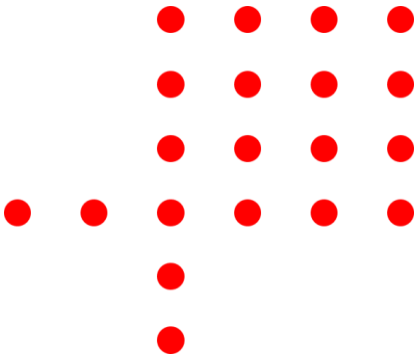

Fig. 19 Thermocouple Placement in Grid

The test was conducted only orienting the heat gun within the first quadrant with the assumption of equal performance in other quadrants. When rotating the heat gun, the exhaust was controlled to not go past the farthest thermocouple. This ensured the exhaust stream was entirely captured by the surrounding thermocouples. The front end of the heat gun nozzle was held at a constant distance of 6 inches from the front of the thermocouple grid. During the test, the heat gun was first held in a non-rotated orientation to allow for the origin point to be set and for the exhaust stream to heat up. Next, the heat gun was rotated up and held at that position. Following this, the heat gun was turned back to the straight orientation and then rotated horizontally. Finally, the heat gun was turned to a diagonal position and then back straight to complete the test. The following figures show the generated animation, paused at the origin and vectored positions. The thermal diffusion shown in Figure 23 may be due to this vectored position having the largest distance between the heat gun and thermocouple grid. However, the analysis code can still easily locate the center of the exhaust stream.

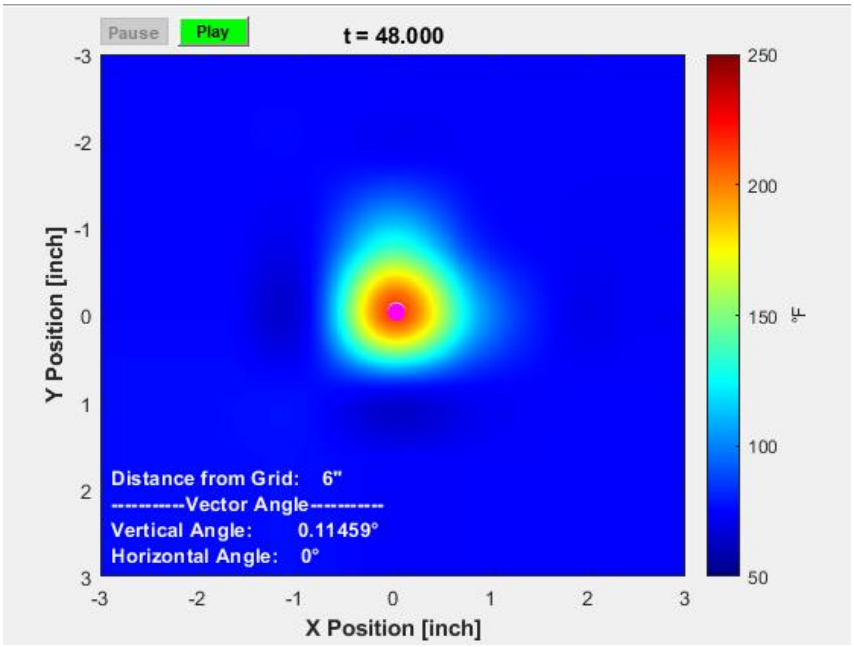

Fig. 20 Thermocouple Grid Animation showing No Vector

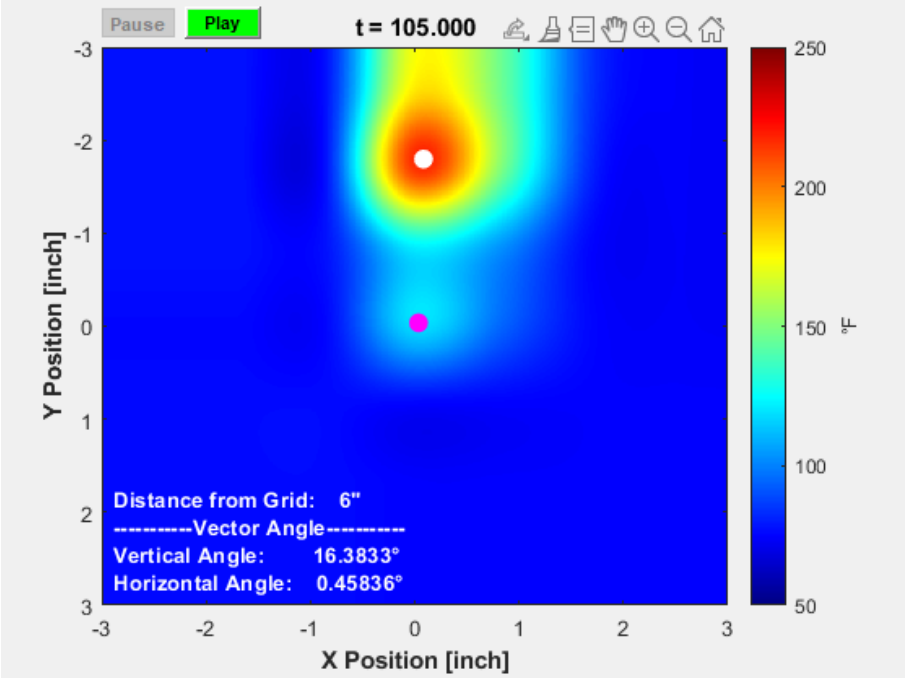

Fig. 21 Thermocouple Grid Animation showing Vertical Vector

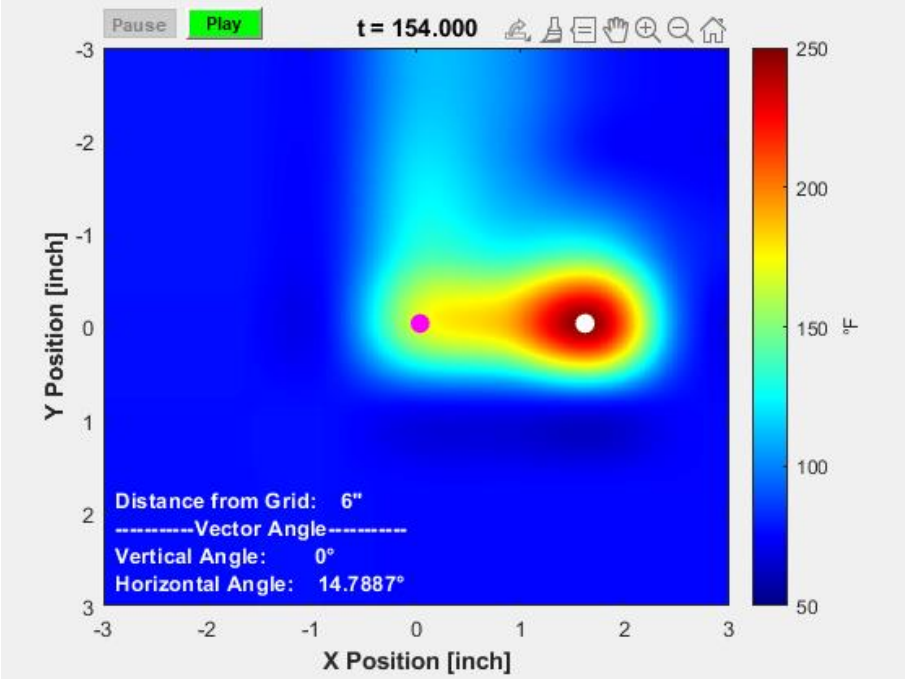

Fig. 22 Thermocouple Grid Animation showing Horizontal Vector

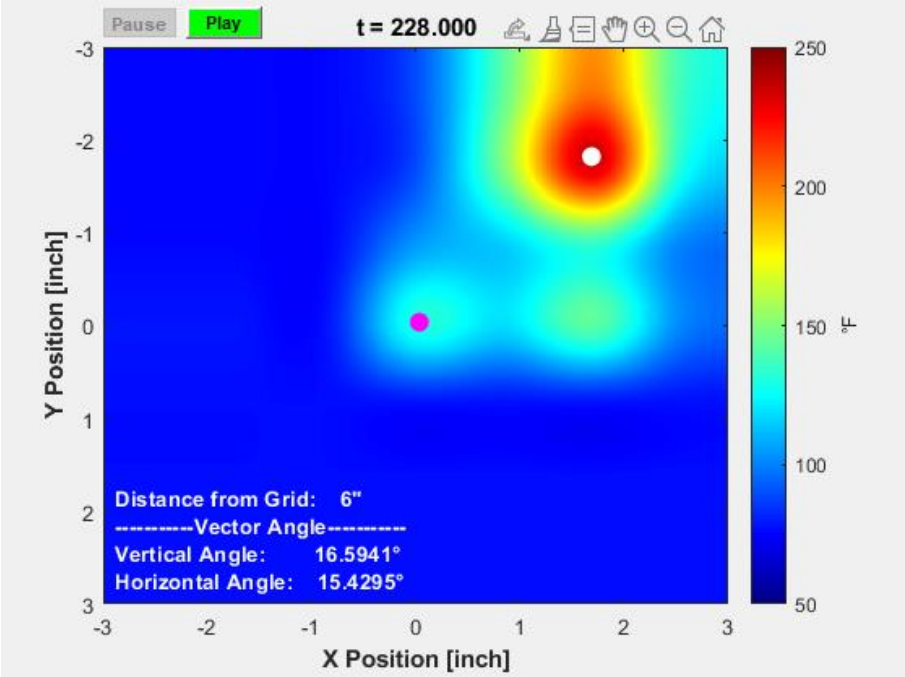

Fig. 23 Thermocouple Grid Animation showing Diagonal Vector

The differences between the thermocouple grid and sensor measurements are provided below in Table 1. For all three rotation types, the difference between the sensor and thermocouple grid was below 8%.

Table. 1 Differences between Sensor and Thermocouple Grid Measurements

	Sensor Measurement(s)	Thermocouple Grid Measurement(s)	Avg. Difference [°, %]
Vertical Angle [°]	17.61	16.27	**1.34°, 7.61%**
Horizontal Angle [°]	16	14.79	**1.21°, 7.56%**
Diagonal Angle (Vert., Hor.) [°]	18.61, 16	16.48, 15.43	**1.35°, 7.8%**

VII. Assumptions and Sources of Error

Several assumptions were made for this study. First, there was be an expectation that the exhaust gas stream is concentrated within a small spatial area on the thermocouple grid and circular, so that the stream is easily discernible from the ambient by temperature. Based on the experimental results, this assumption is validated. Additionally, hot spots were expected in the exhaust, caused by uneven fuel injection and combustion. Uneven heat in the exhaust stream would complicate finding the geometric center of the stream. However, the hot stream was assumed to be contained within a small area, still allowing for the exhaust position to be located. This assumption is left unvalidated as tests using the gas turbine engine were not possible. Therefore, exhaust from engine combustion was not tested. Furthermore, one possible cause of error was cooling of the exhaust gas stream by the ambient air. This heat transfer would cause the temperature gradient between the exhaust and ambient to be less visible, complicating the location of the exhaust stream for analysis. However, preliminary results have shown a temperature difference of over 500 °F between the exhaust stream and the neighboring ambient air. Therefore, cooling should not be an issue, as the expected temperature difference will be too large to cool rapidly. This assumption is also validated as the heat gun did not have thermal diffusion issues either, despite the fact that the heat gun exhaust stream is about 250 °F less than the exhaust of the JetCat P100 engine. Also, two sources of error are sensors used to measure vector angles for verification. The iPhone compass application is only valid to the nearest degree, thus fractional degrees of rotation are not captured. In addition, the digital protractor has an accuracy of 0.05°. Through the course of testing the thermocouple measurement system in the revised experimental setup, the increased need for higher thermocouple resolution became evident. Due to the limited spatial distribution of the thermocouples, the heat gun could only be vectored about 15° to completely capture the exhaust stream. Therefore, in future implementation of this system, for more measurement adaptability, more thermocouples should be used to allow for higher vector angles and for more measurement resolution within the grid.

VIII. Conclusion

This study has provided documentation on a non-traditional thrust vector measurement method. The improvised system experiment proved to be within 8% of physical observations. Therefore, initial results for the use of thermocouples for measurement have proven that this method may be a possible viable alternative for testing needs. The benefits of a thermocouple measurement system are the significant cost reductions, in comparison to the standard load cell method, as well as accuracies within 8%. In conclusion, this research has explored the viability of thermocouple-based thrust vector measurement for a possible cost advantage in engine testing applications.

IX. Acknowledgements

I would like to thank Mr. Karl Roush for his critical contributions to this study as an author. I would also like to thank Mr. Andrew Yatsko for his extensive support and guidance throughout this research project. In addition, I would like to thank Mr. Jonathan Blevins and Mr. Christopher Perullo for reviewing my abstract and providing important feedback. Furthermore, I would like to thank the 2019/20 APOP student team for being so helpful and dedicated. This study is made possible by the Georgia Institute of Technology Aerospace Systems Design Laboratory, Dr. Dimitri Mavris, and Dr. Jimmy Tai. In addition, I would like to thank the Air Force Research Laboratory for hosting the Aerospace Propulsion Outreach Program.

X. References

[1] Ünal, A., Yaman, K., Okur, E., and Adlı, M. A., "Design and Implementation of a Thrust Vector Control (TVC) Test System," Journal of Polytechnic, Oct. 2018.

[2] Nunn, R., & Naval Postgraduate School Monterey Ca. (1988). *TVC (Thrust Vector Control) Jet Vane Thermal Modeling Using Parametric System Identification.*

[3] Buonanno, A., Drikakis, Papachristou, Savvaris, Vamvakoulas, & Warsop. (2010). Computational investigation of the DEMON unmanned air vehicle thrust vectoring system. *Proceedings of the Institution of Mechanical Engineers, Part G: Journal of Aerospace Engineering, 224(4),* 387-394. doi:10.1243/09544100JAERO569.

[4] Solomon, R., Moore, A., Dicus, J., Burns, M., Sheer, I., Bryant, L., & Block, H. (1988). Techniques utilized in the simulated altitude testing of a 2D-CD vectoring and reversing nozzle - NASA-TM-100872.

[5] Almuhsen Al-Asady, Ali Abdul, and Ahmed Mujahid Abdullah. "Fluidics Thrust Vectoring Using Co-Flow Method." Al-Nahrain Journal for Engineering Science vol. 20, no. 1, 2017, pp. 5–18.

[6] Eriksson, A., Lindegren, R., & Kohler, J. (2005). A dynamic millinewton thrust vector measurement system in silicon. *13th International Conference on Solid-State Sensors, Actuators and Microsystems*, IEEE 2005. Digest of Technical Papers. TRANSDUCERS '05, 1, 547-550 Vol. 1.

[7] Jun Zhang, Baoyuan Sun, Zongjin Ren, & Yue Liu. (2009). Research on the Measurement of Thrust Vector for a Liquid-Propellant Rocket Motor Based on Piezoelectric Quartz. *2009 International Conference on Measuring Technology and Mechatronics Automation*, IEEE, 338-341.

[8] Omega, "Miniature Load Cell 2" diameter All Stainless Steel with Back Mounting Holes," Omega Engineering Inc, 2020.

[9] National Instruments, "NI-9237 C Series Strain/Bridge Input Module," National Instruments, 2020.

[10] Omega, "Ready-Made Insulated Thermocouples with Kapton®, PFA, Glass Braid Insulation and Molded Connectors," Omega Engineering Inc, 2020.

[11] National Instruments, "NI-9210 C Series Temperature Input Module," National Instruments, 2020.

[12] National Instruments, "NI-9213 C Series Temperature Input Module," National Instruments, 2020.

[13] Chief Aircraft, "P100-RX Turbine Engine, 22.5 lbs Thrust, by JetCat," Chief Aircraft Inc, 2020.

[14] Hennecke, C., Von der Haar, H., and Dinkelacker, F., "Failure Detection in an Annular Combustion Chamber with Experimental and Numerical Methods," Journal of Aeronautics & Aerospace Engineering, vol. 06, 2017, p. 1.

[15] Hasburgh, L., Bourne, K., Peralta, P., Mitchell, P., Schiff, S., and Pang, W., "Effect of Adhesives and Ply Configuration on the Fire Performance of Southern Pine Cross-Laminated Timber," 2016.

[16] Gall, E., "Heatmaps in Matlab for plotting time-series particle size distributions," May 2015.